HHS Public Access

Author manuscript

Biochemistry. Author manuscript; available in PMC 2021 June 17.

Published in final edited form as:

Biochemistry. 2021 April 13; 60(14): 1088–1096. doi:10.1021/acs.biochem.1c00152.

The Crystal Structure of Calmodulin Bound to the Cardiac Ryanodine Receptor (RyR2) at Residues Phe4246–Val4271 Reveals a Fifth Calcium Binding Site

Qinhong Yu, **David E. Anderson**, **Ramanjeet Kaur**

Department of Chemistry, University of California, Davis, California 95616, United States

Andrew J. Fisher,

Department of Chemistry and Department of Molecular and Cellular Biology, University of California, Davis, California 95616, United States;

James B. Ames

Department of Chemistry, University of California, Davis, California 95616, United States;

Abstract

Calmodulin (CaM) regulates the activity of a Ca^{2+} channel known as the cardiac ryanodine receptor (RyR2), which facilitates the release of Ca^{2+} from the sarcoplasmic reticulum during excitation–contraction coupling in cardiomyocytes. Mutations that disrupt this CaM-dependent channel inactivation result in cardiac arrhythmias. RyR2 contains three different CaM binding sites: CaMBD1 (residues 1940–1965), CaMBD2 (residues 3580–3611), and CaMBD3 (residues 4246–4275). Here, we report a crystal structure of Ca^{2+}-bound CaM bound to RyR2 CaMBD3. The structure reveals Ca^{2+} bound to the four EF-hands of CaM as well as a fifth Ca^{2+} bound to CaM in the interdomain linker region involving Asp81 and Glu85. The CaM mutant E85A abolishes the binding of the fifth Ca^{2+} and weakens the binding of CaMBD3 to Ca^{2+}-bound CaM. Thus, the binding of the fifth Ca^{2+} is important for stabilizing the complex in solution and is not a crystalline artifact. The CaMBD3 peptide in the complex adopts an α-helix (between Phe4246 and Val4271) that interacts with both lobes of CaM. Hydrophobic residues in the CaMBD3 helix (Leu4255 and Leu4259) form intermolecular contacts with the CaM N-lobe, and the CaMBD3 mutations (L4255A and L4259A) each weaken the binding of CaM to RyR2. Aromatic residues on the opposite side of the CaMBD3 helix (Phe4246 and Tyr4250) interact with the CaM C-lobe, but the mutants (F4246A and Y4250A) have no detectable effect on CaM binding in solution. We suggest that the binding of CaM to CaMBD3 and the binding of a fifth Ca^{2+} to CaM may contribute to the regulation of RyR2 channel function.

Corresponding Author: **James B. Ames** – Department of Chemistry, University of California, Davis, California 95616, United States; Phone: (530) 752-6358; jbames@ucdavis.edu; Fax: (530) 752-8995.

Author Contributions

Q.Y. and D.E.A. contributed equally to this work. J.B.A. designed research and, with input from other authors, wrote the paper. Q.Y., D.E.A., R.K., A.J.F., and J.B.A. performed research. Q.Y., D.E.A., A.J.F., and J.B.A. analyzed data.

The authors declare no competing financial interest.

Accession Codes

Atomic coordinates for the CaM/CaMBD3 complex, PDB entry 7KL5.

Complete contact information is available at: https://pubs.acs.org/10.1021/acs.biochem.1c00152

Graphical Abstract

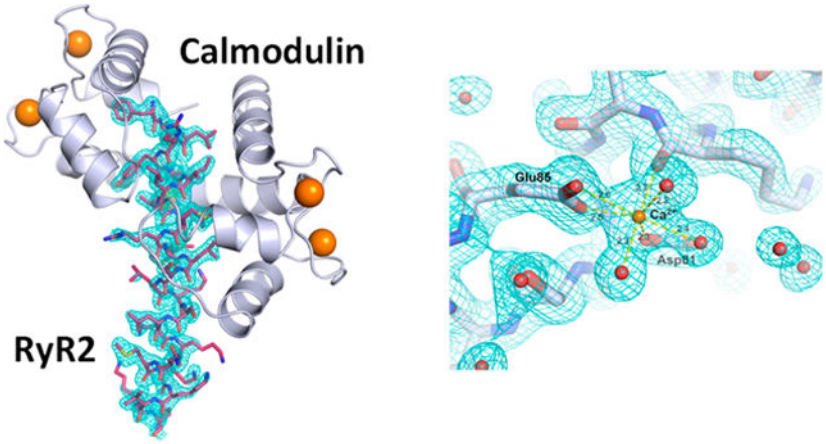

The cardiac ryanodine receptor (RyR2) is a 5.6 MDa ion channel that controls the release of Ca^{2+} from the sarcoplasmic reticulum (SR) in cardiac cells.[1] The excitation of cardiac cells activates RyR2, which initiates a process known as Ca^{2+}-induced Ca^{2+} release (CICR) that in turn leads to the contraction of myofilaments.[2] RyR2 forms homotetrameric channels with a central channel domain and a large cytosolic domain that binds to Ca^{2+}, CaM, and other regulatory proteins.[3–5] RyR2 channel activity is regulated by the intracellular Ca^{2+} concentration in a biphasic fashion.[1,2,6] Under basal conditions at low cytosolic Ca^{2+} levels (0.1 μM), the RyR2 channel remains closed. Intermediate Ca^{2+} levels (0.1–1.0 μM) cause the RyR2 channel to open, whereas increased Ca^{2+} levels (>1.0 μM) cause channel inactivation mediated by CaM. CaM binds to RyR2 and prevents the release of Ca^{2+}, in a process known as CaM-dependent inactivation.[3,7–9] CaM consists of four EF-hand Ca^{2+} binding motifs that are grouped into two domains (N-lobe and C-lobe) connected by a linker, which enables the N-lobe and C-lobe to contact separate target binding sites.[10–12] The CaM-dependent inactivation of RyR2 is important for the replenishment of the SR Ca^{2+} stores following their depletion during cardiomyocyte excitation.[1,2] Mutations in CaM that disrupt CaM-dependent inactivation of RyR2 are genetically linked to cardiac arrhythmias.[7,8,13–16]

Previous studies[17,18] showed that CaM can bind to three distinct sites within RyR2: CaMBD1 (residues 1940–1965), CaMBD2 (residues 3580–3611), and CaMBD3 (residues 4246–4275) (Figure 1). Atomic level structures have been determined for CaM bound to CaMBD2,[19,20] but no such structures are known for CaM bound to CaMBD1 or CaMBD3. In this study, we present the X-ray crystal structure of CaM bound to CaMBD3 (Figure 1). The structure reveals the two lobes of CaM wrap around a central helix of the CaMBD3 peptide, and the intermolecular contacts are mostly hydrophobic. Ca^{2+} is bound to CaM in each of the four EF-hands in the familiar open conformation. A fifth Ca^{2+} is bound to CaM near the interdomain linker. The crystal structure of the CaM/CaMBD3 complex may provide new insights into the regulation of RyR2 by Ca^{2+}-dependent association with channel accessory proteins.

MATERIALS AND METHODS

Protein Expression and Purification.

Construction, expression, and purification of CaM and mutants were performed as described previously.[12,21] The CaM E85A mutation was introduced by site-directed mutagenesis, using wild-type human CaM cDNA in expression vector pET11b as the template, and the following primers: 5′-GATAGCGAAG-AAGCCATTCGTGAAGCG-3′ and 5′-CGCTTCACGA-ATGGCTTCTTCGCTATC-3′. The mutation was confirmed by Sanger sequencing. Recombinant CaM protein was expressed using the pET11b-CaM construct in BL-21(DE3) cells at 37 °C in Luria broth. Cell pellets were resuspended in 20 mM Tris-HCl (pH 7.5), 50 mM KCl, and 2 mM EGTA, incubated with 0.2 mg/mL lysozyme and 0.2 mM phenyl-methanesulfonyl fluoride for 30 min in 4 °C, and then sonicated. The cellular extract was applied to a hydrophobic interaction column [HiPrep Phenyl FF (High Sub) 16/10] equilibrated with high-Ca^{2+} binding buffer [20 mM Tris-HCl (pH 7.5), 200 mM KCl, and 2 mM $CaCl_2$]. The apoCaM protein was eluted from the column using low-Ca^{2+} elution buffer [20 mM Tris-HCl (pH 7.5), 50 mM KCl, and 2 mM EGTA]. The eluate containing apoCaM was then applied to an anion exchange column (HiPrep Q FF 16/10) equilibrated with binding buffer [20 mM Tris-HCl (pH 7.5), 50 mM KCl, and 2 mM EGTA]. The apoCaM protein was isolated from the anion exchange column using a KCl gradient that varied from 20 mM to 0.5 M over 10 column volumes. The final purified CaM protein was concentrated to 20 mg/mL. The CaMBD3 peptide (FALRYNILTLMRMLSLKSLKKQMKKVKKMTV) was purchased from GenScript.

X-ray Crystallography of the CaM/CaMBD3 Complex.

The CaM/CaMBD3 complex used for crystallization trials was prepared by adding 1.34 mL of a CaM stock solution (20 mg/mL) to 50 mL of a stirring solution of 10 mM Tris-HCl (pH 8.0), 1 M KCl, and 1 mM $CaCl_2$. The CaMBD3 peptide powder (8.6 mg) was dissolved in 1.0 mL of water and added dropwise to the CaM solution while it was being stirred. The mixture, with a 1.35:1 CaMBD3:CaM molar ratio, was concentrated to a final volume of 0.44 mL (60 mg/mL) and served as a stock solution for crystallization screenings. The best crystal was grown by the hanging drop method at 4 °C in two to three months after equal volumes of the protein complex and crystallization solution [0.2 M sodium acetate, 0.1 M Tris (pH 8.5), and 30% (w/v) PEG 4000] had been mixed. Before being flash-cooled, the crystal was transferred for several minutes into a cryoprotectant solution containing the mother liquor and 30% ethylene glycol.

X-ray diffraction data were collected at the APS synchrotron on beamline 24-ID-E. Diffraction data were integrated using XDS[22] and scaled with AIMLESS.[23] The CaM/CaMBD3 complex structure was determined by molecular replacement searching for separate N-lobe and C-lobe calmodulin domains [Protein Data Bank (PDB) entry 2bcx] without the ryanodine receptor peptide[19] for a phasing model, using PHASER.[24] The initial electron density map clearly revealed the presence of the CaMBD3 peptide binding to CaM. The structure was modeled into the electron density map using COOT[24] and refined using REFMAC.[25] The data collection and refinement statistics are summarized in Table 1.

Atomic coordinates and structure factors are deposited in the Protein Data Bank (entry 7KL5).

Fluorescence Polarization Binding Assay.

Fluorescein-labeled peptides were purchased from Genscript (Piscataway, NJ). Individual reaction conditions (in a 384-well plate format) consisted of 100 nM peptide in FP buffer [50 mM HEPES (pH 7.3), 100 mM KCl, 1 mM $MgCl_2$, and 2.0 mM $CaCl_2$] and increasing concentrations of the appropriate purified CaM variant. After the solution had been mixed and incubated at room temperature for approximately 30 min, fluorescence polarization was measured with a Synergy 2 plate reader (BioTek, Winooski, VT). To generate binding curves and obtain K_d values, data were fitted in Microsoft Excel to a one-site binding model [$Y = [L]/(K_d + [L])$], using the method of least squares.

NMR Spectroscopy of the CaM/CaMBD3 Complex.

Samples of CaM and the CaM/CaMBD3 complex for NMR analysis were prepared by exchanging the protein complex (^{15}N-labeled Ca^{2+}-bound CaM bound to unlabeled CaMBD3 peptide) into a buffer containing 20 mM Tris-d_{11} (pH 7.5) with 1 mM $CaCl_2$, 100 mM KCl, and 92% H_2O/8% D_2O. In the NMR sample of the complex, the concentrations of ^{15}N-labeled CaM and unlabeled CaMBD3 peptide were 0.3 and 0.5 mM, respectively. All NMR experiments were performed at 30 °C on a Bruker Avance 800 MHz spectrometer equipped with a four-channel interface and a triple-resonance cryogenic (TCI) probe. The ^{15}N–^{1}H HSQC spectrum (Figure 4) was recorded with 256 and 2048 complex points for ^{15}N(F1) and ^{1}H(F2), respectively.

Isothermal Titration Calorimetry (ITC).

The binding of Ca^{2+} to the CaM/CaMBD3 complex (and CaM^{E85A}/CaMBD3) was measured on a VP-ITC calorimeter (Micro-Cal) at 27 °C as described previously.[26,27] The ITC titration buffer contained 20 mM Tris (pH 7.5) and 100 mM KCl. The concentration of the CaM/CaMBD3 complex in the sample cell was 10 μM, and the Ca^{2+} concentration in the injection syringe was 350 μM. The sample was titrated with 35 injections of 7 μL aliquots. Data analysis and fitting was performed using Origin (OriginLab).

ICP-MS Analysis of Ca^{2+} Concentration.

Inductively coupled plasma mass spectrometry (ICP-MS) analysis was performed on separate samples of the CaM^{WT}/CaMBD3 and CaM^{E85A}/CaMBD3 complexes [1.2 mL of 193 μM protein in 10 mM Tris (pH 7.5)] to quantify the number of Ca^{2+} ions bound to each complex in solution. Each protein sample was dialyzed against 2 L of dialysis buffer [40 μM $CaCl_2$ and 10 mM Tris (pH 7.5)], which set the equilibrium free Ca^{2+} concentration of each protein sample to approximately 40 μM and supplied Ca^{2+} to bind to each protein complex. An aliquot (1.2 mL) of each dialyzed protein sample and dialysis buffer blank was digested with 120 μL of concentrated HNO_3 (Fisher Scientific) by heating at 95 °C for 3 h, followed by the addition of 10% H_2O_2 and additional incubation for 1.5 h at 95 °C. The digested protein samples, dialysis buffer blank, and digestion batch QC samples, external standards, and blanks were sampled using an Agilent SPS 4 Autosampler equipped with a 0.25 mm

inside diameter sample probe, mixed at an 18:1 ratio with a custom internal standard solution using a mixing tee, and introduced into the Agilent 8900 ICP-MS instrument (Agilent Technologies, Palo Alto, CA) via a peristaltic pump at 0.10 rps using a 0.4 mL/min MicroMist nebulizer to produce an aerosol in a 2 °C temperature-controlled double pass spray chamber leading to a 1550 W plasma. The custom internal standard solution with Sc, Ge, Y, In, and Bi was diluted from Inorganic Ventures (Inorganic Ventures, Inc., Christiansburg, VA) single-element standards to 7.5 ppm of each element. External standards were diluted from a custom Inorganic Ventures multielement standard mix containing Ca to 100, 1000, and 10000 ppb, and the Ca calibration range was extended to 100 and 200 ppm using the SPEX CertiPrep CS3 standard. The ICP-MS instrument was tuned and calibrated prior to analysis and operated in MS/MS mode using a three-point peak pattern with three replicates per injection and 50 sweeps per replicate with a 0.3 s integration time for Ca and other monitored masses, and 0.1 s integration times for the internal standard masses. Helium mode was used in the collision/reaction cell during the measurements to reduce the level of polyatomic interference. NIST 1640a Trace Elements in Natural Water and a blank were analyzed initially for independent source QC calibration and blank verification. The custom Inorganic Ventures multielement standard mix was analyzed at 100 and 1000 ppb, and the SPEX CertiPrep CS3 standard was analyzed at 10 ppm along with a blank as quality controls before and after the digested protein samples, dialysis buffer blank, and digestion batch QC samples to monitor instrument performance and provide continuing calibration and blank verification. The raw data were processed using MassHunter ICP-MS software (G7201C, version C.01.03, Agilent), and a correction equation was used to remove doubly charged Sr interference from the raw Ca signal.

RESULTS

Crystal Structure of CaM Bound to RyR2 CaMBD3 (residues 4246–4275).

Atomic level structures have been determined for CaM bound to a peptide derived from the RyR1 CaMBD2 sequence,[19] but no such structures are known for CaM bound to CaMBD1 or CaMBD3. We initially tried to crystallize CaM bound to RyR2 CaMBD1, but diffraction quality crystals of the CaM/CaMBD1 complex so far have remained elusive, perhaps due to the relatively low affinity of the complex. By contrast, diffraction quality crystals were successfully formed for Ca^{2+}-bound CaM bound to a 30-residue peptide derived from RyR2 CaMBD3 (Figure 1). The X-ray crystal structure of the CaM/CaMBD3 complex is shown in Figure 2 (data processing and refinement statistics are listed in Table 1). Representative electron density maps that reveal a fifth Ca^{2+} binding site of the CaM/CaMBD3 complex are shown (Figure 2A) along with an omit difference electron density map confirming the well-defined electron density for three water ligands and an electron dense calcium ion (Figure 2B). An electron density map of the bound CaMBD3 peptide is shown in Figure 2C.

In the crystal structure of the CaM/CaMBD3 complex (Figure 2), CaM forms a collapsed structure in which the two lobes of CaM (N-lobe in light blue and C-lobe in darker blue in Figure 2D) each contact the opposite sides of the CaMBD3 target helix (colored red in Figure 2D). The four EF-hands in CaM are each bound to Ca^{2+} and adopt the familiar open conformation.[28] A fifth Ca^{2+} is bound to CaM in the interdomain linker region that includes

residues Asp81 and Glu85 (Figure 2A,B). The fifth Ca^{2+} ion is coordinated by both carboxylate oxygens of Glu85, one carboxylate oxygen from Asp81, and the main chain carbonyl oxygen of Lys78, together with three water molecules in a pentagonal bipyramid geometry. The temperature *B*-factor for the fifth calcium ion (33.7 $Å^2$) is comparable to those of the four other calcium ions in the EF-hands (average of 33.4 $Å^2$). CaMBD3 in the complex adopts a 24-residue α-helix (residues 4246–4270, colored red in Figures 1 and 2). The last five residues at the C-terminus of CaMBD3 (residues 4271–4275) are not visible in the electron density map. Hydrophobic residues in the CaMBD3 helix (Ile4252, Leu4255, Met4256, and Leu4259) each make intermolecular contacts with residues in the CaM N-lobe (Figure 2E). Aromatic residues (Phe4246 and Tyr4250) on the opposite side of the CaMBD3 helix make intermolecular contacts with residues in the CaM C-lobe (Figure 2F). Mutagenesis studies below verify that residues Leu4255 and Leu4259 are both important for the binding of the CaM N-lobe to CaMBD3.

RyR2 Mutants (L4255A and L4259A) Weaken the Binding of RyR2 to the CaM N-Lobe.

The crystal structure of the CaM/CaMBD3 complex identifies key hydrophobic amino acid residues at the binding interface between RyR2 and the CaM N-lobe (Figure 2E). CaMBD3 residues (Leu4255 and Leu4259) that interact with the CaM N-lobe were mutated to Ala to form the following mutants of the CaMBD3 peptide: L4255A and L4259A. To evaluate the effects of the CaMBD3 mutations on CaM N-lobe binding, we performed fluorescence polarization (FP) binding assays as described previously[17] (Figure 3A). The FP binding data reveal that the wild-type RyR2 CaMBD3 peptide binds to the Ca^{2+}-bound CaM N-lobe construct (residues 1–78, called CaMN) with a dissociation constant (K_d) of 200 ± 50 nM. The CaMBD3 peptide mutants L4255A and L4259A bind to the Ca^{2+}-bound CaMN with K_d values of 400 ± 50 and 450 ± 50 nM, respectively. The weaker binding observed here for each mutant is consistent with these residues forming intermolecular contacts with the CaM N-lobe in the crystal structure (Figure 2E).

RyR2 Mutants (F4246A and Y4250A) Do Not Affect the Binding of CaM to RyR2.

The crystal structure of the CaM/CaMBD3 complex identifies aromatic residues (Phe4246 and Tyr4250) at the binding interface between RyR2 and the CaM C-lobe (Figure 2F). These CaMBD3 residues were mutated to Ala to form the CaMBD3 mutants: F4246A and Y4250A. To evaluate the effects of these mutations on CaM C-lobe binding, we performed FP binding assays as described previously[17] (Figure 3B). The FP binding data reveal that the wild-type RyR2 CaMBD3 peptide binds to the Ca^{2+}-bound CaM C-lobe construct (residues 82–149, called CaMC) with a dissociation constant (K_d) of 400 ± 50 nM. The CaMBD3 peptide mutants F4246A and Y4250A each bind to the Ca^{2+}-bound CaMC with the same K_d as that of the wild type. Our binding analysis indicates that the F4246A and Y4250A mutants do not affect the binding of RyR2 to CaMC in solution. This result suggests that the interaction of the CaM C-lobe with Phe4246 and Tyr4250 (shown in Figure 2F) might somehow be different from the interaction probed by the FP binding assay in solution (Figure 3B). Analysis of NMR spectra of 15N-labeled CaM bound to unlabeled CaMBD3 peptide in solution (Figure 4) reveals that the chemical shifts of many residues from the CaM C-lobe (G97, I101, A103, G114, T118, D119, I131, G133, Q136, V137, N138, and A148 shown labeled in Figure 4) are not affected much by the presence of CaMBD3. This is

in contrast to a larger chemical shift perturbation of residues from the CaM N-lobe (L19, F20, I28, A29, T30, G34, and G41) caused by the binding of CaMBD3. The smaller chemical shift perturbation for residues in the CaM C-lobe is consistent with its weaker binding to CaMBD3 compared to that of the N-lobe (Figure 3), which may explain why the F4246A and Y4250A mutations have no detectable effect on the binding of RyR2 to the CaM C-lobe (Figure 3B). Because RyR2 residues Phe4246 and Tyr4250 are both not conserved in other types of ryanodine receptors (RyR1 and RyR3),[17] the intermolecular contacts with Phe4246 and Tyr4250 (Figure 2F) may not be biologically important.

Because the RyR2 mutations (F4246A and Y4250A) have no detectable effect on CaMC binding, we wanted to test whether CaMC in solution might bind to a different site in CaMBD3 compared to the site bound to the C-lobe of full-length CaM (Figure 2F). In solution and in the absence of an N-lobe, CaMC could perhaps bind to the opposite side of the CaMBD3 helix occupied by the CaM N-lobe (Figure 2E). A similar competitive binding between CaMC and CaMN was seen for CaMBD2.[17] To test this possibility in CaMBD3, we measured the binding of CaMC to the CaMBD3 double mutant (L4255A/L4259A) that causes 4-fold weaker binding to CaMN (Figure 3A, green). The CaMBD3 double mutant (L4255A/L4259A) also causes weaker binding to CaMC (Figure 3B, green), suggesting that CaMC in solution (and in the absence of the N-lobe) may bind competitively to the same site in CaMBD3 that binds to CaMN (Figure 2E). To further test this idea, an HSQC NMR spectrum was recorded for ^{15}N-labeled CaMC bound to the unlabeled CaMBD3 peptide (Figure 4, green peaks). Many of the resolved resonances of CaMC have similar chemical shifts compared to the corresponding resonances in full-length CaM (Figure 4, black peaks). However, a number of other CaMC resonances (assigned to E83, I86, L117, G134, and N138) have detectably different chemical shifts compared to the corresponding resonances in full-length CaM. These spectral differences are consistent with CaMC perhaps binding to a different site in CaMBD3 compared to the site bound to the C-lobe from full-length CaM (Figure 2F). Interestingly, the largest spectral differences are assigned to residues (E83 and I86) located near the fifth Ca^{2+} binding site in full-length CaM that must not exist in CaMC bound to CaMBD3, because the fifth site is comprised of residues in the domain linker that are missing in CaMC.

A Fifth Ca^{2+} Binds to the CaM Interdomain Linker in the CaM/CaMBD3 Complex.

The crystal structure (Figure 2D) reveals a fifth Ca^{2+} is bound to the interdomain linker region of CaM involving Asp81 and Glu85 in the CaM/CaMBD3 complex that is not normally bound to CaM alone. Isothermal titration calorimetry (ITC) experiments were performed to evaluate the binding energetics of this fifth Ca^{2+} (Figure 5). The ITC isotherm for the binding of Ca^{2+} to the CaM^{WT}/CaMBD3 complex (Figure 5A) illustrates a Ca^{2+} binding stoichiometry of five Ca^{2+} ions bound per CaM molecule in the complex, because a significant heat signal is still detected when the molar ratio (Ca^{2+}:CaM) along the horizontal axis is increased from 4 to 5. Accordingly, the ITC isotherm in Figure 5A was best fit by a five-site model (see Table 2 for binding parameters). The binding analysis reveals that four Ca^{2+} ions bind to the EF-hand motifs with relatively high affinity (K_1 and K_2 = 100 nM, and K_3 and K_4 = 1.0 μM), and an extra fifth Ca^{2+} binds to the CaM/CaMBD3 complex in the micromolar range (K_5 = 5.0–50.0 μM). Thus, as expected from the crystal structure (Figure

2D), the CaM/CaMBD3 complex in solution exhibits a total of five Ca^{2+} ions bound per CaM molecule in the presence of a saturating level of CaMBD3. To test whether Glu85 is essential for binding the fifth Ca^{2+} (Figure 2D), we constructed the CaM mutant (CaM^{E85A}) in which Glu85 was mutated to Ala. This mutant is expected to significantly weaken the binding of the fifth Ca^{2+}, because both carboxylate oxygens of Glu85 coordinate to the fifth Ca^{2+}. The ITC isotherm for the binding of Ca^{2+} to the CaM^{E85A}/CaMBD3 complex (Figure 5B) suggests a Ca^{2+} binding stoichiometry of four Ca^{2+} ions bound per CaM^{E85A} molecule in the complex, because the heat signal in the isotherm nearly goes to zero when the molar ratio (Ca^{2+}:CaM) is greater than 4. When this isotherm (Figure 5B) is fit with a five-site model, the K_5 value must be greater than 10^{-3} M to allow the isotherm to saturate near a molar ratio of 4. This implies that the fifth site in the CaM^{E85A}/CaMBD3 complex has at least 100-fold weaker binding affinity compared to that of the wild type. As a negative control, a Ca^{2+} binding stoichiometry of four Ca^{2+} ions per CaM molecule was measured for CaM^{E85A} in the absence of CaMBD3 (Figure 5C). The Ca^{2+} binding dissociation constants for the four EF-hands of CaM^{E85A} in the absence of CaMBD3 (see K_1–K_4 in Table 2) are nearly identical to those of wild-type CaM,[30] which demonstrates that the E85A mutation does not affect the binding of Ca^{2+} to the four EF-hands. In summary, the ITC data reveal a total of four Ca^{2+} ions bound per CaM^{E85A} molecule with a relatively high affinity, and a fifth Ca^{2+} in the micromolar range is not detected to bind to the CaM^{E85A}/CaMBD3 complex. This analysis indicates that the E85A mutation significantly weakens the binding of a fifth Ca^{2+} in the domain linker region. In addition, the E85A mutation causes a 2-fold weaker binding of full-length Ca^{2+}-bound CaM to CaMBD3 (Figure 3C). Thus, the binding of the fifth Ca^{2+} appears to stabilize the CaM/CaMBD3 complex at physiological Ca^{2+} concentrations, suggesting that the fifth site is not a crystalline artifact.

A Fifth Ca^{2+} Bound to the CaM/CaMBD3 Complex Detected by ICP-MS.

Inductively coupled plasma mass spectrometry (ICP-MS) analysis was performed on samples of both CaM^{WT}/CaMBD3 and CaM^{E85A}/CaMBD3 complexes to quantify the number of Ca^{2+} ions bound to each complex in solution. Separate samples of CaM^{WT}/CaMBD3 and CaM^{E85A}/CaMBD3 complexes [1.2 mL of 193 ± 10 μM protein complex dissolved in 10 mM Tris (pH 7.5)] were each dialyzed against 2 L of dialysis buffer [40 μM $CaCl_2$ and 10 mM Tris (pH 7.5)]. The total Ca^{2+} concentration of each dialyzed sample was measured by ICP-MS to be 0.90 ± 0.02 mM (CaM^{WT}/CaMBD3) and 0.81 ± 0.02 mM (CaM^{E85A}/CaMBD3) (Figure 6). The free Ca^{2+} concentration was measured by ICP-MS to be 39.0 ± 1 μM (derived from ICP-MS analysis of the dialysis buffer blank in Figure 6). The bound Ca^{2+} concentration (total Ca^{2+} concentration minus free Ca^{2+} concentration) was calculated to be 0.86 ± 0.02 mM for the CaM^{WT}/CaMBD3 complex and 0.77 ± 0.02 mM for the CaM^{E85A}/CaMBD3 complex. The number of Ca^{2+} ions bound to each protein complex (bound Ca^{2+} concentration divided by the protein concentration) was calculated to be 4.5 ± 0.1 Ca^{2+} ions bound to each molecule of the CaM^{WT}/CaMBD3 complex, compared to 4.0 ± 0.1 Ca^{2+} ions bound to each molecule of the CaM^{E85A}/CaMBD3 complex. The ICP-MS analysis reveals a 50% occupancy of a fifth Ca^{2+} bound to the CaM^{WT}/CaMBD3 complex in solution (free Ca^{2+} concentration of 39.0 μM), consistent with a fifth Ca^{2+} site seen in the crystal structure (Figure 2D). The 50% occupancy of the lowest-affinity fifth site of the CaM^{WT}/CaMBD3 complex (when the free Ca^{2+} concentration is 39.0 μM) implies a

dissociation constant of ~39.0 μM for the fifth site, which is in the same range measured by ITC (see K_5 in Table 2).

DISCUSSION

The binding of CaM to RyR2 facilitates rapid channel inactivation at elevated cytosolic Ca^{2+} levels following the excitation of cardiac cells.[9] Mutations in CaM that disrupt CaM-dependent channel inactivation are genetically linked to cardiac arrhythmias.[7,8,13,14] A recent cryo-EM study revealed the structure of RyR2 bound to CaM in a closed channel state (at low cytosolic Ca^{2+} levels) and in the Ca^{2+}-activated open state.[5] In the cryo-EM structures of both RyR1/CaM[31] and RyR2/CaM[5] complexes, CaM is bound to only CaMBD2 (residues 3581–3611), while CaMBD3 (residues 4246–4275) is not resolved. Therefore, the atomic level structure of RyR2 CaMBD3 bound to CaM has remained unknown. In this study, we present the X-ray crystal structure of CaM bound to a peptide derived from CaMBD3 (Figure 2). The two lobes of CaM wrap around a central helix of the CaMBD3 peptide, which is reminiscent of the crystal structures of CaM bound to RyR1 CaMBD2[19] and RyR2 CaMBD2.[20] An important structural difference is a fifth Ca^{2+} bound to the CaM/CaMBD3 complex (Figure 2A) that is not detected in the CaM/CaMBD2 complex. Also, the CaMBD3 residue Leu4259 makes critical hydrophobic contacts with the CaM N-lobe (Figure 2E), whereas the homologous residue in CaMBD2 (Gln3627) is solvent-exposed and does not make intermolecular contacts in the CaM/CaMBD2 complex. This structural difference may explain why the CaM N-lobe binds with a 10-fold higher affinity to CaMBD3 than to CaMBD2.[17]

Previous electrophysiology studies of RyR2[32] and the recent cryo-EM structure of RyR2 bound to CaM[5] indicate that the binding of CaM to CaMBD2 alone may be sufficient to promote CaM-dependent channel inactivation.[33] Thus, binding of CaM to CaMBD3 is not required for CaM-dependent channel inactivation of RyR2. If CaMBD3 is not important for channel inactivation, then what is the physiological role of the binding of CaM to CaMBD3? Binding of CaM to CaMBD3 might alternatively mediate the Ca^{2+}-dependent association of ryanodine receptors with various accessory proteins that regulate channel function.[33] For example, the RyR2 accessory protein CaM-dependent protein kinase II (CaMKII) exhibits Ca^{2+}-dependent association with RyR2[34,35] that might be influenced by the binding of CaM to CaMBD3. In addition, CaM might mediate the Ca^{2+}-dependent association of ryanodine receptors (RyR1 and RyR2) with voltage-gated L-type Ca^{2+} channels ($Ca_V1.1$ and $Ca_V1.2$).[36–38] In particular, the binding of CaM to CaMBD3 could possibly facilitate the Ca^{2+}-induced coupling between RyR1 and $Ca_V1.1$.[33,39] Indeed, a key residue in RyR1 (E4242) that is required for coupling to $Ca_V1.1$ is located very close to CaMBD3,[39] and the amino acid residues in CaMBD3 that contact the CaM N-lobe are highly conserved in both RyR1 and RyR2.[17] We suggest that the association of ryanodine receptors with L-type channels might require binding of the high-affinity CaM N-lobe to CaMBD3 (Figure 2E), along with binding of the CaM C-lobe to the IQ motif in the L-type Ca^{2+} channel.[38,40,41] In essence, the two CaM lobes are proposed here to structurally connect RyR1 with $Ca_V1.1$ (or RyR2 with $Ca_V1.2$). The preferential binding of the CaM N-lobe to RyR (and the CaM C-lobe to the L-type channel) is supported by the observation that the CaM N-lobe binds to CaMBD3 with an affinity (Figure 3A) higher than that with which it binds to the L-type channel,[42]

while the CaM C-lobe binds to the L-type channel[42] with an affinity higher than that with which it binds to CaMBD3 (Figure 3B). A similar bridging of two separate sites by the CaM lobes was also seen in the structures of the TRPV6/CaM[43] and TRPV5/CaM complexes.[44] Future studies that abolish the binding of CaM to CaMBD3 in full-length ryanodine receptors (e.g., CaMBD3 deletion or L4255A/L4259A mutation within full-length RyR2) are needed to test whether the binding of CaM to CaMBD3 is required for Ca^{2+}-induced association of RyRs with L-type Ca^{2+} channels or other RyR-associated proteins.

The crystal structure of the CaM/CaMBD3 complex reveals the binding of a fifth Ca^{2+} to CaM (Figure 2B) that is not observed in the absence of CaMBD3 (Figure 5). A previous crystal structure of CaM reported a fifth bound Ca^{2+} that mediates a crystal contact between Glu47 and Asp58.[45] This fifth site is most likely a consequence of the close packing of the crystalline environment and was concluded to have no biological importance.[45] By contrast, the binding of a fifth Ca^{2+} to the CaM/CaMBD3 complex observed in this study does not involve any crystalline contacts, is detected in solution by ITC and ICP-MS, and has a sufficiently high affinity [K_5 = 5.0–50.0 μM (Figure 5 and Table 2)] to occur under physiological conditions. Also, the binding of the fifth Ca^{2+} causes a 2-fold increase in the binding affinity of the CaM/CaMBD3 complex (Figure 3C), which might be important for fine-tuning the stability of the CaM/RyR2 complex under physiological conditions. Future experiments are needed to determine whether disabling the binding of this fifth Ca^{2+} [using the CaM^{E85A} mutation (see Figure 3C)] would have any effect on RyR2 channel function.

ACKNOWLEDGMENTS

The authors thank Jeff Walton and Ping Yu for help with NMR experiments and Austin M. Cole for help with ICP-MS experiments. The ICP-MS experiments were performed at the UC Davis Interdisciplinary Center for Plasma Mass Spectrometry, using an Agilent model 8900 ICP-MS instrument purchased with funding from the UC Davis Research Core Facility Enhancement Funding Program managed by the UC Davis Office of Research. This work is based upon research conducted at the Northeastern Collaborative Access Team beamlines, which are funded by the National Institute of General Medical Sciences of the National Institutes of Health (P30 GM124165). The Eiger 16M detector on beamline 24-ID-E is funded by a NIH-ORIP HEI grant (S10OD021527). This research used resources of the Advanced Photon Source, a U.S. Department of Energy (DOE) Office of Science User Facility operated for the DOE Office of Science by Argonne National Laboratory under Contract DE-AC02-06CH11357.

Funding

This work was supported by National Institutes of Health Grant R01-EY012347 to J.B.A. A.J.F. is partially supported by U.S. Department of Agriculture National Institute of Food and Agriculture Hatch Grant CA-D-MCB-2629-H.

ABBREVIATIONS

CaM	calmodulin
FP	fluorescence polarization
HSQC	heteronuclear single-quantum coherence
ICP-MS	inductively coupled plasma mass spectrometry
ITC	isothermal titration calorimetry
RyR1	ryanodine receptor from skeletal muscle

RyR2	ryanodine receptor from cardiac cells

REFERENCES

(1). Fearnley CJ, Roderick HL, and Bootman MD (2011) Calcium signaling in cardiac myocytes. Cold Spring Harbor Perspect. Biol 3, a004242.

(2). Bers DM (2008) Calcium cycling and signaling in cardiac myocytes. Annu. Rev. Physiol 70, 23–49. [PubMed: 17988210]

(3). Van Petegem F (2015) Ryanodine receptors: allosteric ion channel giants. J. Mol. Biol 427, 31–53. [PubMed: 25134758]

(4). Van Petegem F (2019) Slaying a giant: Structures of calmodulin and protein kinase a bound to the cardiac ryanodine receptor. Cell Calcium 83, 102079. [PubMed: 31522075]

(5). Gong D, Chi X, Wei J, Zhou G, Huang G, Zhang L, Wang R, Lei J, Chen SRW, and Yan N (2019) Modulation of cardiac ryanodine receptor 2 by calmodulin. Nature 572, 347–351. [PubMed: 31278385]

(6). Laver DR (2018) Regulation of the RyR channel gating by calcium and magnesium. Biophys. Rev 10, 1087–1095. [PubMed: 29926426]

(7). Sondergaard MT, Tian X, Liu Y, Wang R, Chazin WJ, Chen SR, and Overgaard MT (2015) Arrhythmogenic Calmodulin Mutations Affect the Activation and Termination of Cardiac Ryanodine Receptor-mediated Ca2+ Release. J. Biol. Chem 290, 26151–26162. [PubMed: 26309258]

(8). Sorensen AB, Sondergaard MT, and Overgaard MT (2013) Calmodulin in a heartbeat. FEBS J. 280, 5511–5532. [PubMed: 23663249]

(9). Tian X, Tang Y, Liu Y, Wang R, and Chen SR (2013) Calmodulin modulates the termination threshold for cardiac ryanodine receptor-mediated Ca2+ release. Biochem. J 455, 367–375. [PubMed: 23992453]

(10). Chin D, and Means AR (2000) Calmodulin: aprototypi-calcalcium sensor. Trends Cell Biol. 10, 322–328. [PubMed: 10884684]

(11). VanScyoc WS, Sorensen BR, Rusinova E, Laws WR, Ross JB, and Shea MA (2002) Calcium Binding to Calmodulin Mutants Monitored by Domain-Specific Intrinsic Phenylalanine and Tyrosine Fluorescence. Biophys. J 83, 2767–2780. [PubMed: 12414709]

(12). Zhang Y, Li Z, Sacks DB, and Ames JB (2012) Structural basis for Ca2+-induced activation and dimerization of estrogen receptor a by calmodulin. J. Biol. Chem 287, 9336–9344. [PubMed: 22275375]

(13). Chazin WJ, and Johnson CN (2020) Calmodulin Mutations Associated with Heart Arrhythmia: A Status Report. Int. J. Mol. Sci 21, 1418–1430.

(14). Sondergaard MT, Liu Y, Guo W, Wei J, Wang R, Brohus M, Overgaard MT, and Chen SRW (2020) Role of cardiac ryanodine receptor calmodulin-binding domains in mediating the action of arrhythmogenic calmodulin N-domain mutation N54I. FEBS J 287, 2256–2280. [PubMed: 31763755]

(15). Sondergaard MT, Liu Y, Larsen KT, Nani A, Tian X, Holt C, Wang R, Wimmer R, Van Petegem F, Fill M, Chen SR, and Overgaard MT (2017) The Arrhythmogenic Calmodulin p.Phe142Leu Mutation Impairs C-domain Ca2+ Binding but Not Calmodulin-dependent Inhibition of the Cardiac Ryanodine Receptor. J. Biol. Chem 292, 1385–1395. [PubMed: 27927985]

(16). Walweel K, Oo YW, and Laver DR (2017) The emerging role of calmodulin regulation of RyR2 in controlling heart rhythm, the progression of heart failure and the antiarrhythmic action of dantrolene. Clin. Exp. Pharmacol. Physiol 44, 135–142. [PubMed: 27626620]

(17). Brohus M, Sondergaard MT, Wayne Chen SR, van Petegem F, and Overgaard MT (2019) Ca(2+)-dependent calmodulin binding to cardiac ryanodine receptor (RyR2) calmodulin-binding domains. Biochem. J 476, 193–209. [PubMed: 30530841]

(18). Lau K, Chan MM, and Van Petegem F (2014) Lobe-specific calmodulin binding to different ryanodine receptor isoforms. Biochemistry 53, 932–946. [PubMed: 24447242]

(19). Maximciuc AA, Putkey JA, Shamoo Y, and Mackenzie KR (2006) Complex of calmodulin with a ryanodine receptor target reveals a novel, flexible binding mode. Structure 14, 1547–1556. [PubMed: 17027503]

(20). Holt C, Hamborg L, Lau K, Brohus M, Sorensen AB, Larsen KT, Sommer C, Van Petegem F, Overgaard MT, and Wimmer R (2020) The arrhythmogenic N53I variant subtly changes the structure and dynamics in the calmodulin N-terminal domain, altering its interaction with the cardiac ryanodine receptor. J. Biol. Chem 295, 7620–7634. [PubMed: 32317284]

(21). Turner M, Anderson DE, Nieves-Cintron M, Bartels P, Coleman AM, Yarov V, Bers DM, Navedo MF, Horne MC, Ames JB, and Hell JW (2020) a-Actinin-1 promotes gating of the L-type Ca2+ Channel CaV1.2. EMBO J. 39, e102622. [PubMed: 31985069]

(22). Kabsch W (2010) Xds. Acta Crystallogr., Sect. D: Biol. Crystallogr 66, 125–132. [PubMed: 20124692]

(23). Evans PR, and Murshudov GN (2013) How good are my data and what is the resolution? Acta Crystallogr., Sect. D: Biol. Crystallogr 69, 1204–1214. [PubMed: 23793146]

(24). Abba MC, Hu Y, Sun H, Drake JA, Gaddis S, Baggerly K, Sahin A, and Aldaz CM (2005) Gene expression signature of estrogen receptor alpha status in breast cancer. BMC Genomics 6, 37. [PubMed: 15762987]

(25). Murshudov GN, Skubak P, Lebedev AA, Pannu NS, Steiner RA, Nicholls RA, Winn MD, Long F, and Vagin AA (2011) REFMAC5 for the refinement of macromolecular crystal structures. Acta Crystallogr., Sect. D: Biol. Crystallogr 67, 355–367. [PubMed: 21460454]

(26). Lim S, Peshenko IV, Dizhoor AM, and Ames JB (2009) Effects of Ca2+, Mg2+, and myristoylation on guanylyl cyclase activating protein 1 structure and stability. Biochemistry 48, 850–862. [PubMed: 19143494]

(27). Lim S, Scholten A, Manchala G, Cudia D, Zlomke-Sell SK, Koch KW, and Ames JB (2017) Structural Characterization of Ferrous Ion Binding to Retinal Guanylate Cyclase Activator Protein 5 from Zebrafish Photoreceptors. Biochemistry 56, 6652–6661. [PubMed: 29172459]

(28). Babu YS, Bugg CE, and Cook WJ (1988) Structure of calmodulin refined at 2.2 A resolution. J. Mol. Biol 204, 191–204. [PubMed: 3145979]

(29). Chen VB, Arendall WB 3rd, Headd JJ, Keedy DA, Immormino RM, Kapral GJ, Murray LW, Richardson JS, and Richardson DC (2010) MolProbity: all-atom structure validation for macromolecular crystallography. Acta Crystallogr., Sect. D: Biol. Crystallogr 66, 12–21. [PubMed: 20057044]

(30). Gilli R, Lafitte D, Lopez C, Kilhoffer M, Makarov A, Briand C, and Haiech J (1998) Thermodynamic analysis of calcium and magnesium binding to calmodulin. Biochemistry 37, 5450–5456. [PubMed: 9548926]

(31). Woll KA, Haji-Ghassemi O, and Van Petegem F (2021) Pathological conformations of disease mutant Ryanodine Receptors revealed by cryo-EM. Nat. Commun 12, 807. [PubMed: 33547325]

(32). Yamaguchi N, Xu L, Pasek DA, Evans KE, and Meissner G (2003) Molecular basis of calmodulin binding to cardiac muscle Ca(2+) release channel (ryanodine receptor). J. Biol. Chem 278, 23480–23486. [PubMed: 12707260]

(33). Meissner G (2017) The structural basis of ryanodine receptor ion channel function, The. J. Gen. Physiol 149, 1065–1089. [PubMed: 29122978]

(34). Bers DM (2004) Macromolecular complexes regulating cardiac ryanodine receptor function. J. Mol. Cell. Cardiol 37, 417–429. [PubMed: 15276012]

(35). Zhang T, Maier LS, Dalton ND, Miyamoto S, Ross J Jr., Bers DM, and Brown JH (2003) The deltaC isoform of CaMKII is activated in cardiac hypertrophy and induces dilated cardiomyopathy and heart failure. Circ. Res 92, 912–919. [PubMed: 12676814]

(36). Rios E, and Brum G (1987) Involvement of dihydropyridine receptors in excitation-contraction coupling in skeletal muscle. Nature 325, 717–720. [PubMed: 2434854]

(37). Stroffekova K (2008) Ca2+/CaM-dependent inactivation of the skeletal muscle L-type Ca2+ channel (Cav1.1). Pfluegers Arch. 455, 873–884. [PubMed: 17899167]

(38). Stroffekova K (2011) The IQ motif is crucial for Cav1.1 function. J. Biomed. Biotechnol 2011, 504649. [PubMed: 22162637]

(39). Bannister RA, Sheridan DC, and Beam KG (2016) Distinct Components of Retrograde Ca(V)1.1-RyR1 Coupling Revealed by a Lethal Mutation in RyR1. Biophys. J 110, 912–921. [PubMed: 26910427]

(40). Halling DB, Georgiou DK, Black DJ, Yang G, Fallon JL, Quiocho FA, Pedersen SE, and Hamilton SL (2009) Determinants in CaV1 channels that regulate the Ca2+ sensitivity of bound calmodulin. J. Biol. Chem 284, 20041–20051. [PubMed: 19473981]

(41). Van Petegem F, Chatelain FC, and Minor DL Jr. (2005) Insights into voltage-gated calcium channel regulation from the structure of the CaV1.2 IQ domain-Ca^{2+}/calmodulin complex. Nat. Struct. Mol. Biol 12, 1108–1115. [PubMed: 16299511]

(42). Evans TI, Hell JW, and Shea MA (2011) Thermodynamic linkage between calmodulin domains binding calcium and contiguous sites in the C-terminal tail of Ca(V)1.2. Biophys. Chem 159, 172–187. [PubMed: 21757287]

(43). Singh AK, McGoldrick LL, Twomey EC, and Sobolevsky AI (2018) Mechanism of calmodulin inactivation of the calcium-selective TRP channel TRPV6. Sci. Adv 4, eaau6088. [PubMed: 30116787]

(44). Dang S, van Goor MK, Asarnow D, Wang Y, Julius D, Cheng Y, and van der Wijst J (2019) Structural insight into TRPV5 channel function and modulation. Proc. Natl. Acad. Sci. U. S. A 116, 8869–8878. [PubMed: 30975749]

(45). Wilson MA, and Brunger AT (2000) The 1.0 A crystal structure of Ca(2+)-bound calmodulin: an analysis of disorder and implications for functionally relevant plasticity. J. Mol. Biol 301, 1237–1256. [PubMed: 10966818]

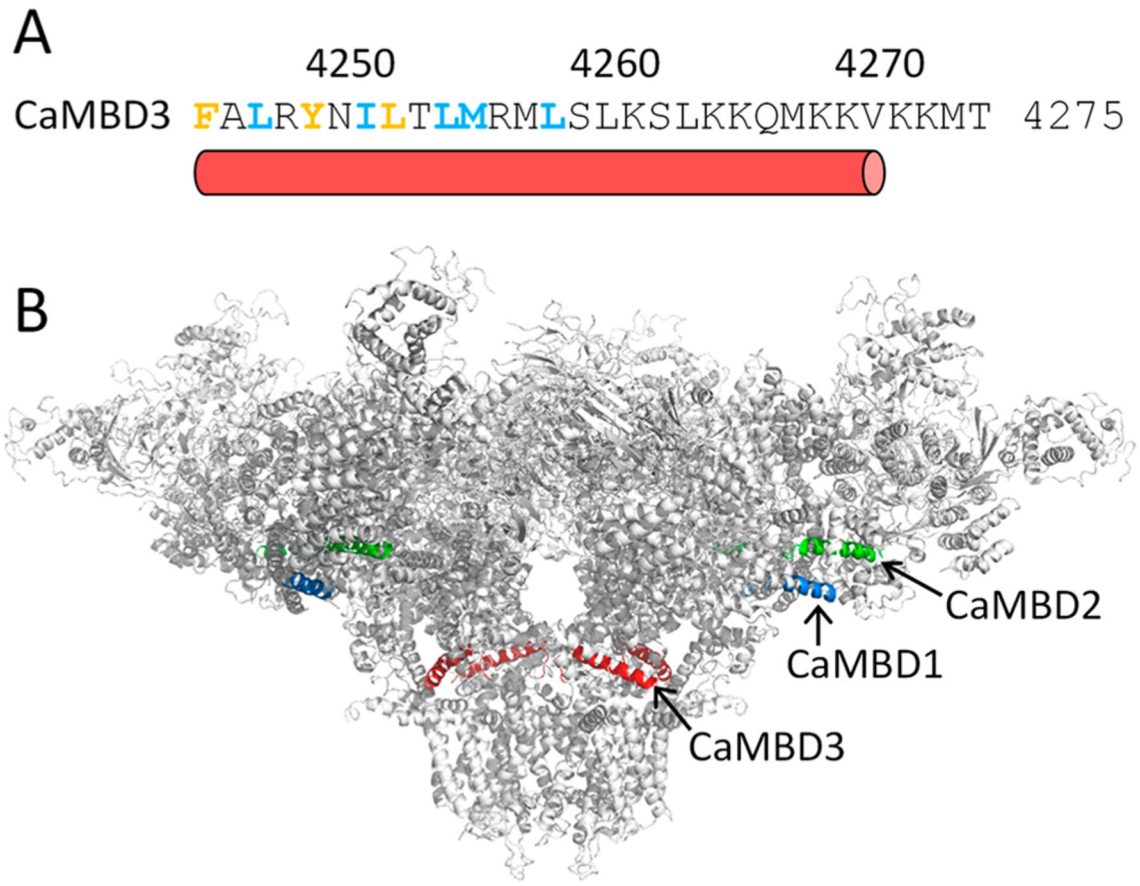

Figure 1.

Amino acid sequence of CaMBD3 and cryo-EM structure of RyR2. (A) Amino acid sequence of CaMBD3 and helical region depicted by a red cylinder. CaMBD3 residues that contact the CaM N-lobe (blue) and CaM C-lobe (orange) are highlighted in bold. (B) Cryo-EM structure of RyR2 (Protein Data Bank entry 6JIY). CaM binding domains are colored.

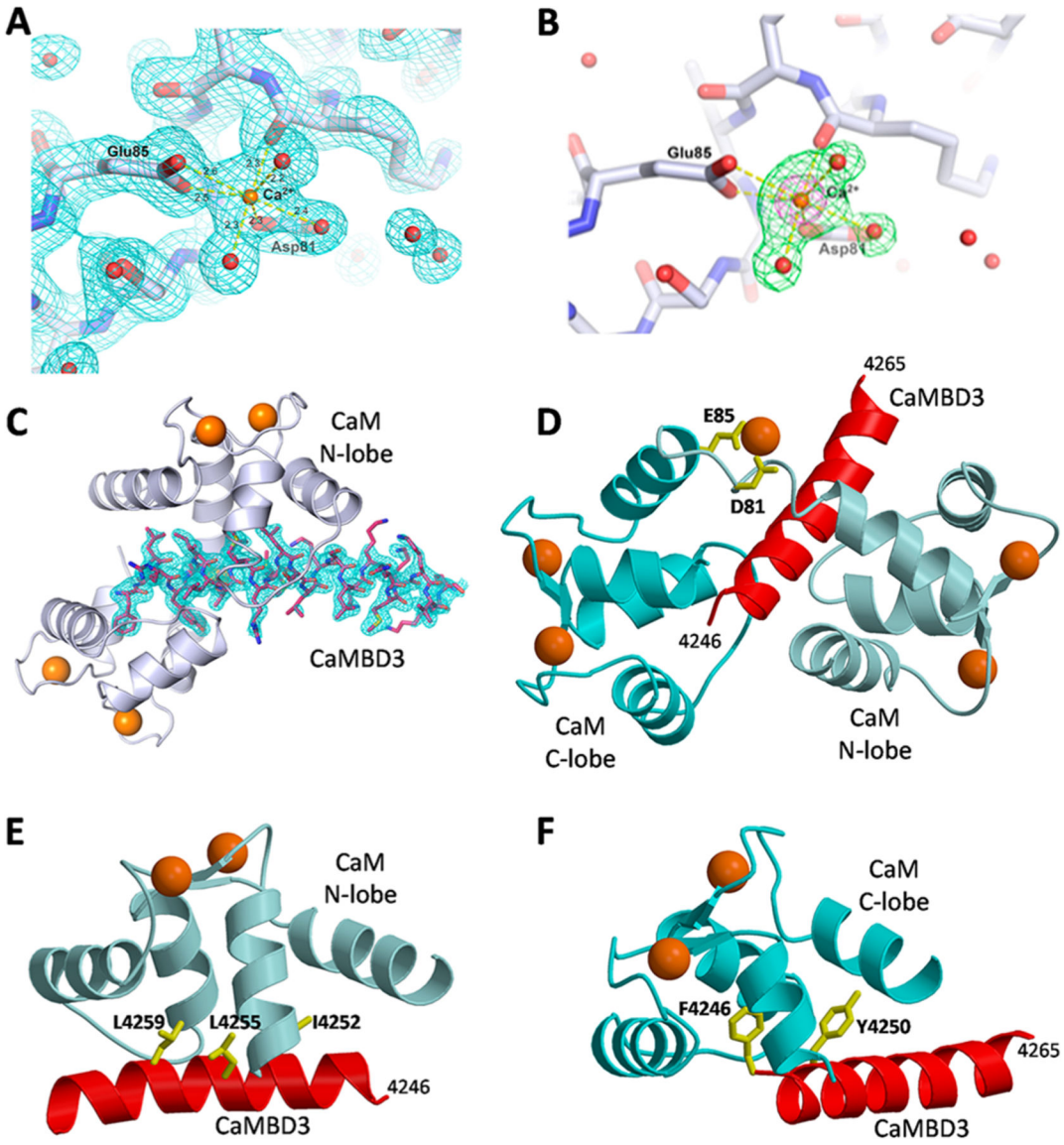

Figure 2.

Crystal structure of the CaM/CaMBD3 complex. (A) Representative $2F_o - F_c$ electron density map of the fifth Ca^{2+} binding site in the CaM/CaMBD3 complex (contoured at 1σ). (B) Omit difference electron density map calculated after the fifth calcium and coordinated waters were deleted and refined. Difference density is contoured at 3σ (green) and 10σ (magenta) shown with the final atomic model. (C) Electron density map of the bound CaMBD3 peptide (contoured at 1σ). (D) Ribbon diagram of the main chain structure of CaM (cyan) bound to the CaMBD3 peptide (red). Bound Ca^{2+} ions (orange) are shown as spheres. (E) Close-up of residues in CaMBD3 (L4255 and L4259) that interact with the CaM N-lobe. (F) Close-up of residues in CaMBD3 (F4246 and Y4250) that interact with the CaM C-lobe. The side chain atoms of CaM residues (D81 and E85) that chelate the bound fifth Ca^{2+} and CaMBD3 residues (L4246, 4250, 4255, and 4259) that interact with CaM are depicted as yellow sticks.

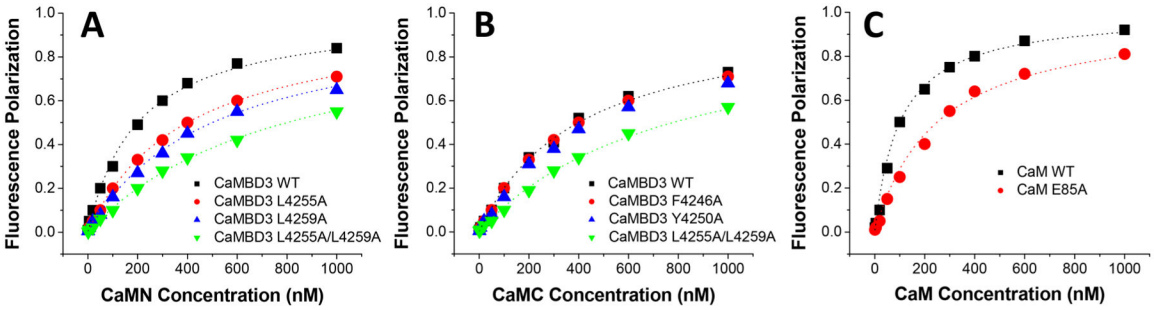

Figure 3.

Fluorescence polarization binding assays. (A) Fractional saturation of the binding of the CaM N-lobe (CaMN) to fluorescently labeled CaMBD3 peptides: wild type (black), L4255A (red), L4259A (blue), and L4255A/L4259A (green). The K_d values are 200 ± 50 nM (wild type), 400 ± 50 nM (L4255A), 450 ± 50 nM (L4259A), and 820 ± 50 nM (L4255A/L4259A). (B) Fractional saturation of the binding of the CaM C-lobe (CaMC) to fluorescently labeled CaMBD3 peptides: wild type (black), F4246A (red), Y4250A (blue), and L4255A/L4259A (green). The K_d values are 400 ± 50 nM (for the wild type, F4246A, and Y4250A) and 850 ± 50 nM (for L4255A/L4259A). (C) Fractional saturation of the binding of fluorescently labeled CaMBD3 peptide to full-length CaM mutants: wild type (black) and E85A (red). The K_d values are 100 ± 50 and 250 ± 50 nM for the wild type and E85A, respectively. Fractional saturation was calculated as $Y = \frac{FP}{FP_{max}\text{-}FP_{min}}$, where FP is the fluorescence polarization, FP_{max} is the maximal FP value at saturation, and FP_{min} is the minimum FP value from the free peptide. Error bars are equal to the symbol size.

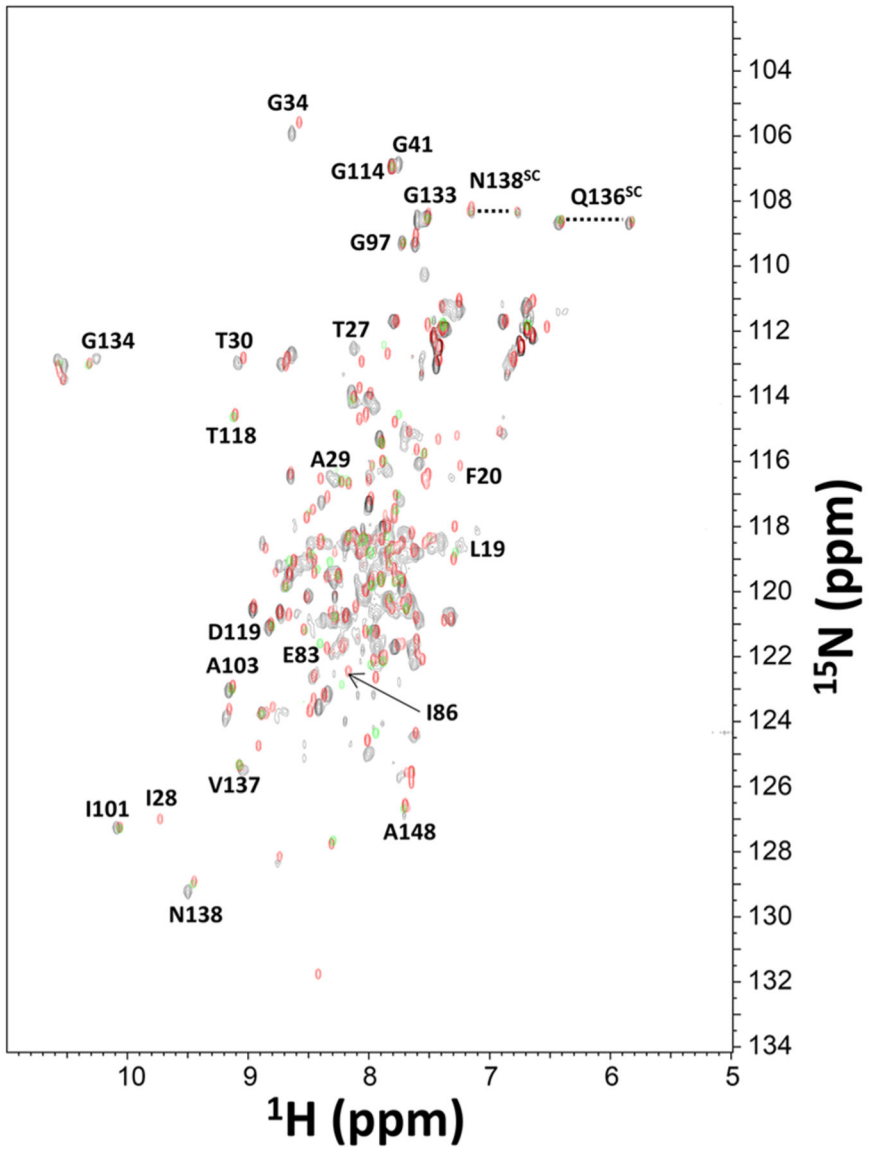

Figure 4.

NMR spectroscopy of the binding of CaM to CaMBD3. ^{15}N–^{1}H HSQC spectra of ^{15}N-labeled Ca^{2+}-bound CaM alone (red) and in the presence of saturating unlabeled CaMBD3 (black) and ^{15}N-labeled Ca^{2+}-bound CaMC bound to CaMBD3 (green). Assignments of resolved residues are marked by residue labels. Assigned side chain amide resonances (designated as $Q135^{SC}$ and $N137^{SC}$) are indicated by the dotted lines. The experimental conditions are defined in Materials and Methods.

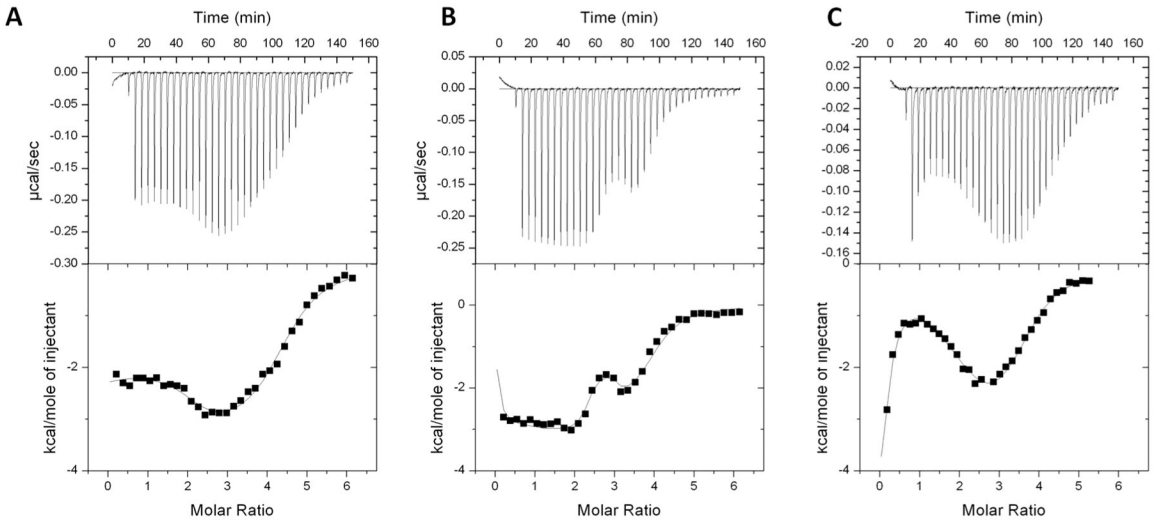

Figure 5.

Isothermal titration calorimetry (ITC) Ca^{2+} binding assays. ITC measurement of the binding of Ca^{2+} to (A) the CaM^{WT}/CaMBD3 complex, (B) the CaM^{E85A}/CaMBD3 complex, and (C) CaM^{E85A} in the absence of CaMBD3. The Ca^{2+} binding isotherms were each fit to a five-site model (solid line). The apparent Ca^{2+} affinity (K_1–K_5) and enthalpy difference (ΔH_1–ΔH_5) for each site are given in Table 2. The experimental conditions are described in Materials and Methods.

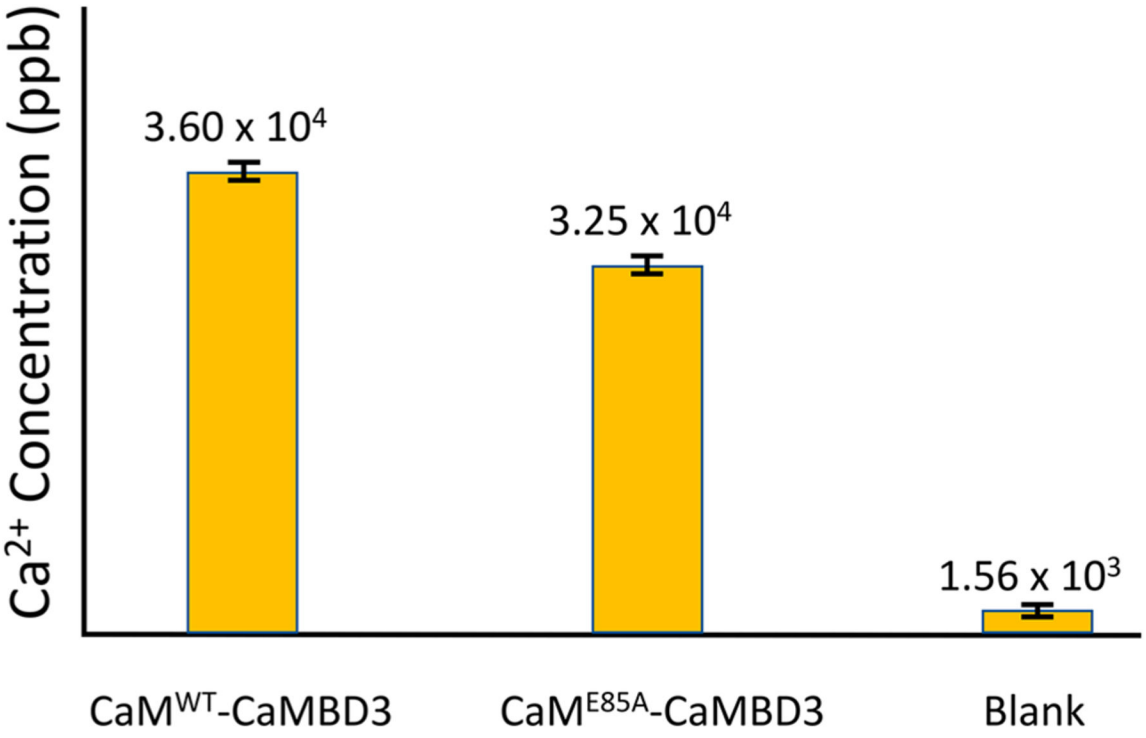

Figure 6.

ICP-MS analysis of Ca^{2+} concentration. Bar graph of the total Ca^{2+} concentration of samples of the CaM^{WT}/CaMBD3 complex (left), the CaM^{E85A}/CaMBD3 complex (center), and a dialysis buffer blank (right). The sample conditions and details of the ICP-MS analysis are described in Materials and Methods.

Table 1.

Data Processing and Refinement Statistics

synchrotron (beamline)	APS (24-ID-E)
wavelength (Å)	0.97918
space group	$P2_1$
unit cell parameters	a = 33.17 Å, b = 62.40 Å, c = 43.19 Å α = 90.0°,β = 107.49°, γ = 90.0°
resolution range (Å)	62.4–1.65 (1.68–1.65)
no. of observed reflections	67125 (3226)
no. of unique reflections	19805 (942)
completeness (%)	97.9 (96.7)
$I/\sigma(I)$	9.3 (1.5)
R_{merge} [a] (%)	5.0 (86.5)
$CC_{1/2}$	99.7 (81.0)
no. of monomers per asymmetric unit	1
Matthews coefficient (Å^3/Da)	2.08
solvent content (%)	40.89
Refinement	
no. of reflections ($F > 0$)	18806
R_{factor} [b] (%)	20.89
R_{free} [b] (%)	24.56
root-mean-square deviation for bond lengths (Å)	0.015
root-mean-square deviation for bond angles (deg)	1.803
coordinate error (Å)	0.120
average B factor (Å^2) (no. of atoms)	
calmodulin	28.5 (1154)
RyR2 peptide	30.6 (241)
calcium ions	33.5 (5)
water	43.2 (72)
ethylene glycols	55.0 (16)
Wilson B factor (Å^2)	30.7
Ramachandran plot [c] (%)	
favored (%)	168 (99.4%)
allowed (%)	1 (0.6%)
outliers (%)	0 (0%)
PDB entry	7KL5

[a] $R_{merge} = \sum_h\sum_i|I_h - I_{hi}|/\sum_h\sum_i I_{hi}$, where I_h is the mean of I_{hi} observations of reflection h. Numbers in parentheses represent values for the highest-resolution shell.

[b] R_{factor} and $R_{free} = \sum||F_{obs}| - |F_{calc}||/\sum|F_{obs}| \times 100$ for 95% of recorded data (R_{factor}) or 5% of the data (R_{free}).

[c] Ramachandran plot statistics from MolProbity.[29]

Table 2.

ITC Thermodynamic Parameters for Binding of Ca^{2+} to the CaM/CaMBD3 Complex[a]

	K_1 (μM)	ΔH_1	K_2 (μM)	ΔH_2	K_3 (μM)	ΔH_3	K_4 (μM)	ΔH_4	K_5 (μM)	ΔH_5
CaM^{WT}	0.1 ± 0.03	−2.3 ± 0.2	0.1 ± 0.03	−2.0 ± 0.2	1.0 ± 0.2	−3.4 ± 0.2	1.0 ± 0.2	−3.0 ± 0.2	5.0–50.0	−1.2 ± 0.1
CaM^{E85A}	<0.1	−10.4 ± 1	<0.1	+4.6 ± 1	0.5 ± 0.3	−1.7 ± 0.4	1.5 ± 0.5	−2.5 ± 0.4	>1000	−1.0 ± 0.2
CaM^{E85A} alone	1.0 ± 0.2	−4.4 ± 0.2	1.1 ± 0.2	+6.4 ± 0.6	2.6 ± 0.5	−1.3 ± 0.5	10.0 ± 1.0	+5.8 ± 0.6	>1000	−1.0 ± 0.2

[a]Dissociation constants (K_i) have units of micromolar. Enthalpy differences (ΔH_i) have units of kilocalories per mole.